Why is Ice Slippery? Simulations of Shear Viscosity of the Quasi-Liquid Layer on Ice

Patrick B. Louden and J. Daniel Gezelter*

251 Nieuwland Science Hall, Department of Chemistry & Biochemistry,

University of Notre Dame, Notre Dame, IN 46556

E-mail: gezelter@nd.edu

Phone: +1 (574) 631-7595

Abstract

The temperature and depth dependence of the shear viscosity (η) of the quasi-liquid layer (QLL) of water on ice-I_h crystals was determined using simulations of the TIP4P/Ice model. The crystals display either the basal $\{0001\}$ or prismatic $\{10\bar{1}0\}$ facets, and we find that the QLL viscosity depends on the presented facet, the distance from the solid / liquid interface, and the undercooling temperature. Structural order parameters provide two distinct estimates of the QLL widths, which are found to range from 6.0-7.8 Å, and depend on facet and undercooling temperature. Above 260 K, the viscosity of the vapor-adjacent water layer is significantly less viscous than the solid-adjacent layer, and is also lower than the viscosity of liquid water.

Graphical TOC Entry

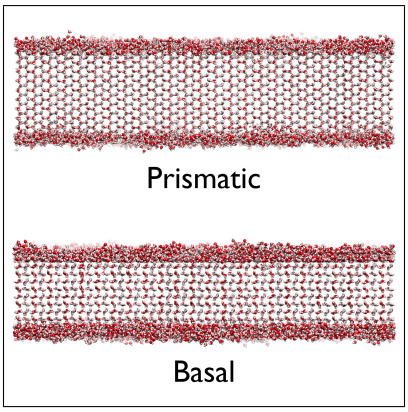

The friction force experienced by a slider moving over the surface of ice is influenced by a quasi-liquid layer (QLL) which mediates the interactions between the ice and the slider. Three regimes of friction on ice have been described: boundary friction, where the lubricating QLL is only a few molecules thick and slider-ice asperities have significant interactions; mixed friction, where the QLL is thicker but some ice-slider interactions remain; and hydrodynamic friction, where the QLL completely supports the slider.[1,2] The width of the QLL is known to be highly sensitive to temperature and pressure, as well as the chemical composition and load of the slider.

In the hydrodynamic friction regime, there are three distinct contributions to the overall observed friction; the solid-liquid friction between the ice and QLL, the viscous shearing of the QLL, and the solid-liquid friction between the QLL and the slider. Recently, we have estimated solid-liquid friction coefficients for four common facets of ice-I_h solvated in bulk water.[3] We observed a differential friction coefficient between the facets, with the prismatic $\{10\bar{1}0\}$ and secondary prismatic $\{11\bar{2}0\}$ displaying larger drag on the liquid than the basal $\{0001\}$ and 14° pyramidal $\{20\bar{2}1\}$ faces. This trend was found to correlate with the density of solid-to-liquid hydrogen bonds at the interface, and a simple model which captured the momentum conductance through the interface was developed. Here, we investigate the temperature dependence of the shear viscosity of the QLL on the basal and prismatic crystal facets. This letter is an attempt to understand the contribution of viscous drag within the thin film of liquid that sits on the surface of ice.

Spontaneous formation of a QLL on the basal and prismatic surfaces was observed at all temperatures investigated (255 K – 270 K). Characterizing this surface premelt has been previously done with a variety of order parameters,[4–12] with the general observation that order parameters decrease as a function of distance from the ice surface, leading to increased mobility of water molecules far from the interface.[4,7] Here, we have chosen two structural parameters, the local density, $\rho(y)$, and the local tetrahedral order parameter, $q(y)$, described by Errington and Debenedetti,[13] and recently renormalized for under- and over-coordinated local structures.[3] To compute profiles of these measures, each of the systems were divided into small bins normal to the interface and an average of the order parameter was computed in that bin. The resulting profiles

for the basal and prismatic systems are presented in Fig. 1.

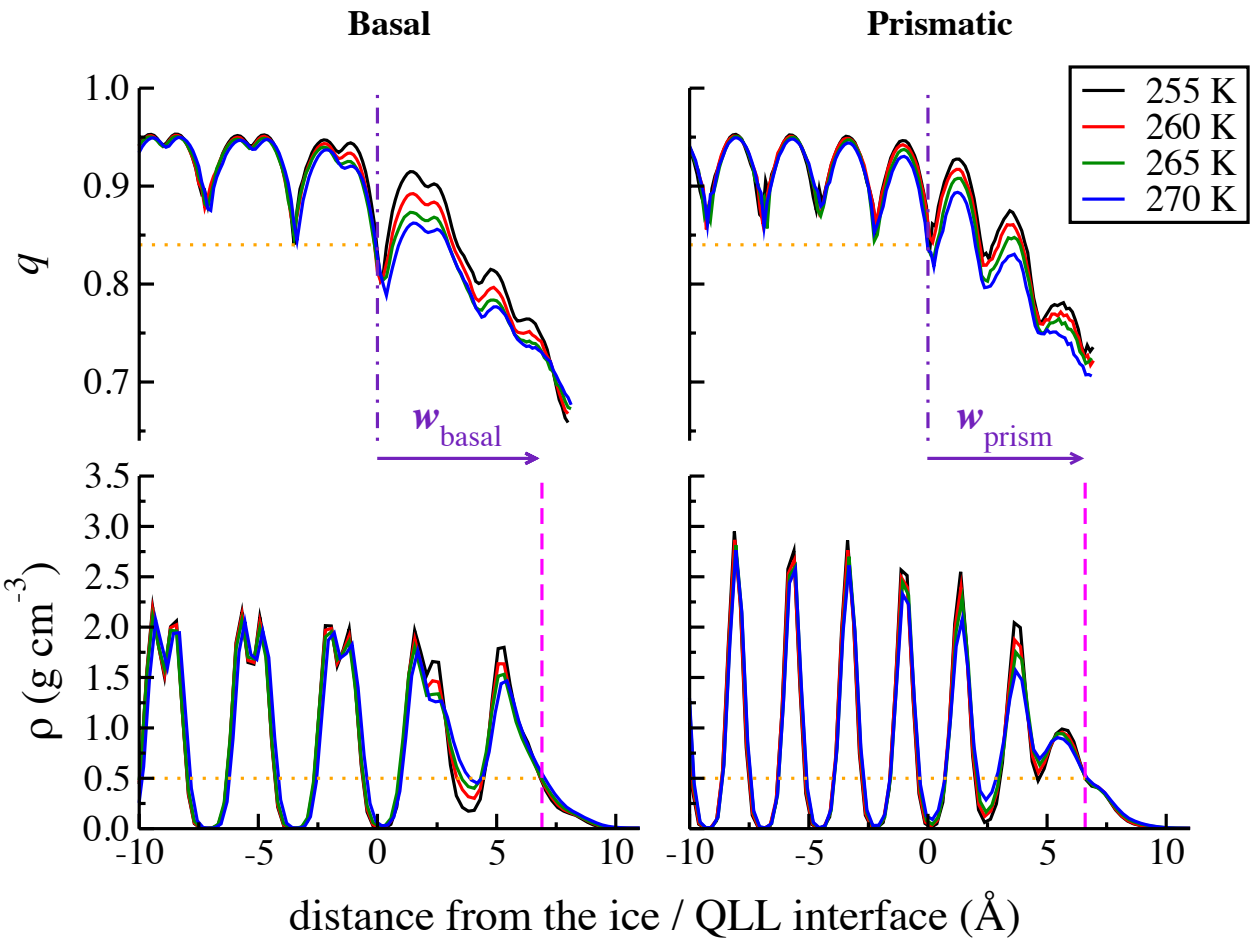

Figure 1: The local density (lower panels) and tetrahedral order parameter (upper panels) of the exposed ice-I_h basal (left) and prismatic (right) facets. Quasi-liquid layer (QLL) formation is observed in the outermost layers (two bilayers for the basal surface, three layers on the prismatic). The position of the QLL / ice interface is referenced to the point where the tetrahedrality q falls below 0.84. The dividing surface for the QLL / vapor interface is set where $\rho = 0.5$ g cm^{-3}.

In the upper panels of Fig. 1, the local tetrahedral order parameter shows the formation of a QLL (right of the purple dashed-dotted line). Interior to the crystal, the crystalline planes have consistent values of $q \sim 0.93$. Previously, we have found $q_{s,l} = 0.84$ to be the solid / liquid dividing surface for ice crystals solvated in bulk water using the same water model.[3] Here, we use $q_{s,l}$ to establish the ice / QLL dividing surface. In the bottom left of this figure, the characteristic bilayer of ice is observed as a series of twin peaks at each plane of ice. The outermost crystal plane has lost the characteristic bilayer, indicating a liquid-like structure. In the prismatic facet (lower right),

the projections of the crystal planes produce single peaks in the density, and we observe loss of tetrahedrality starting in the three outermost layers of water on this interface. In the vapor, small molecular populations prevent calculation of statistically meaningful values of q.

Estimates of the QLL width can be obtained by imposing a dividing surface between the QLL and the vapor where the density goes to $\rho = 0.5$ g cm^{-3}. We define a structural QLL width, w, as the difference in the locations between the ice / QLL tetrahedrality threshold and the QLL / vapor density threshold. We find the QLL width on the basal surface to be $6.8-7.1$ Å, and $6.5-6.7$ Å on the prismatic surface as reported in Table 1.

A second measure for the width of the QLL has been obtained following the method of Conde *et al.*[8] They determined the number of liquid-like molecules,

$$N_{\text{liquid}} = N \int_0^{q_t} p(q) dq, \tag{1}$$

based on a normalized tetrahedrality distribution, $p(q)$, where any molecule with a q smaller than a threshold ($q_t = 0.91$) was counted as a liquid water molecule. The QLL width (δ) is then obtained by relating N_{liquid} to a sample of bulk liquid of equal length and breadth,

$$\delta = \frac{m N_{\text{liquid}}}{2\rho L_x L_z}, \tag{2}$$

where m is the mass of one water molecule and ρ is the bulk density. Our calculations of δ as well as those by Conde *et al.* are reported in Table 1. Note that there are some differences in how the values of δ are computed. Tetrahedrality in this letter has been corrected for under- and over-coordination,[3] so there is no need to remove the population of mis-identified low tetrahedrality molecules using estimates at low temperatures.

The structural QLL widths (w) appear to have low sensitivity to temperature, while the estimates computed from a threshold tetrahedrality (δ) are quite sensitive to undercooling temperature. The computed QLL widths agree with estimates by Conde *et al.*, using the same water potential.[8] These estimates of QLL width also agree with those reported by Nada and Furukawa,[5,6,14]

and Neshyba *et al.*[10–12] Conde has also shown that when compared at the same relative undercooling temperature, the SPC/E, TIP4P, TIP4P/Ice, and TIP4P/2005 models all give similar estimates of QLL width.[8] However, Michaelides and Slater have recently pointed out that there is disagreement in the QLL thickness when measured by X-ray diffraction, X-ray absorption, ellipsometry, and molecular dynamics simulations.[15]

Table 1: Calculated widths of the basal and prismatic quasi-liquid layer (in Å) for the TIP4P/Ice water model. Values for structural widths (w) are computed using the method shown in Fig. 1 while the tetrahedrality-based estimates of QLL width (δ) are computed using Eq. (2). Uncertainties in the last digit are indicated with parentheses.

	This work				Conde *et. al* (Ref. 8)	
Temperature (K)	w_{basal}	w_{prism}	δ_{basal}	δ_{prism}	δ_{basal}	δ_{prism}
255	6.83(6)	6.46(5)	6.03(7)	6.36(1)		
260	6.9(1)	6.49(9)	6.39(5)	6.78(3)		
265	7.1(1)	6.58(9)	7.04(2)	7.21(4)		
266					6.3(4)	5.8(8)
270	7.11(5)	6.69(2)	7.6(3)	7.8(1)	7.5(7)	6.8(8)

The primary quantity of interest in this letter is the shear viscosity, $\eta(y,T)$, of the QLL as a function of both temperature (T) and distance (y) from the ice / QLL interface. The standard molecular dynamics technique for computing viscosities of bulk liquids employs a Green-Kubo relation connecting the time correlation function of the off-diagonal components of the pressure tensor to the shear viscosity. The pressure tensor is a bulk property, so obtaining a spatially-resolved viscosity in the QLL would require local pressure tensor decomposition (e.g. the local stress). However, Vanegas *et al.* showed that different force decomposition methods can result in dramatically varying estimates of lateral stress profiles,[16] so we know of no direct equilibrium simulation method that can accurately provide QLL viscosity profiles.

Measuring a fluid's response to an imposed momentum flux (via non-equilibrium molecular dynamics) is another common route to obtaining shear viscosities. Because the QLL layer is thin, with widely-varying viscosities over the width of the liquid layer, the nonequilibrium methods are statistically challenging. We are instead relying on an indirect measure to estimate the viscosity. The Stokes-Einstein relation, $D = k_B T/6\pi\eta r$, provides an inverse relationship between the diffu-

sion constant and the viscosity of the surrounding medium. Assuming Stokes-Einstein holds with similar boundary conditions for water self-diffusion in both the QLL and the supercooled bulk liquid, we can estimate shear viscosities for the QLL,

$$\eta_{\mathrm{qll}}(y,T) = \frac{D_{\mathrm{bulk}}(T)}{D_{\mathrm{qll}}(y,T)}\eta_{\mathrm{bulk}}(T) \tag{3}$$

The size of the diffusing molecule (r), temperature (T), and consideration of stick/slip boundaries are not present in Eq. (3), as these are assumed to be identical in the QLL and supercooled bulk liquids at the same temperatures. Diffusion constants, spatially resolved along the dimension normal to the ice surface,

$$D_{\mathrm{qll}}(y) = \lim_{t\to\infty}\frac{1}{6t}\left\langle |\mathbf{r}_i(t)-\mathbf{r}_i(0)|^2\,\delta(y_i(0)-y)\delta(y_i(t)-y)\right\rangle, \tag{4}$$

were computed in the QLL. The delta functions sample only those molecules that were present in a thin (1 Å) slab around y during both points of the correlation function. There are some subtleties concerning spatially-resolved bulk diffusion, Eq. (4), vs. two-dimensional diffusion parallel to the ice plane. See the SI for a more detailed discussion of this point.

At the three warmer temperatures investigated here (260, 265, 270 K), the value of $D\eta/T$ remains roughly constant in the bulk supercooled liquids (see Fig. S6 in the Supporting Information). At 255 K, the Stokes-Einstein relation is less well-supported, or the effective hydrodynamic radius may depend on temperature. However, we do not directly invoke the Stokes-Einstein relation to compute viscosities, but rather use the inverse diffusion / viscosity relationship to project from viscosities computed in the bulk. We have separately computed $\eta_{\mathrm{bulk}}(T)$ and $D_{\mathrm{bulk}}(T)$ for each of the temperatures studied to help reduce the decoupling due to temperature when comparing to $D_{\mathrm{qll}}(y,T)$.

Following Eq. (3), each of the spatially resolved diffusion coefficients were compared to bulk simulations done at the same temperature to obtain $\eta(y,T)$ for both the basal and prismatic QLLs. In order to determine $\eta_{\mathrm{bulk}}(T)$ for supercooled liquid water, we have performed velocity shear-

ing and scaling reverse non-equilibrium molecular dynamics (VSS-RNEMD)[17] with simultaneous momentum and kinetic energy fluxes imposed on the same simulation of liquid water. The liquid responds to the imposed fluxes with both thermal and velocity gradients. The magnitudes of the gradients permit calculation of the shear viscosity for supercooled water over a wide range of temperatures. The Supporting Information (SI) provides more details on the simulation protocol. The resulting $\eta_{\text{bulk}}(T)$ values were fit with the Vogel-Fulcher-Tammann (VFT) model, which is widely used to model viscosities of polymers and other liquids which exhibit a glass transition temperature ($T_g \sim 136$ K for water[18]),

$$\eta_{\text{bulk}}(T) = \eta_0 \exp\left(\frac{B}{T - T_0}\right). \tag{5}$$

Here, η_0 and B are parameters describing the infinite temperature viscosity and the thermal energy required to change the viscosity, respectively. T_0 is an empirical parameter, typically taken to be the glass transition temperature (T_g). We have obtained fit values of $\eta_0 \sim 3.6629$ cP, $B \sim 16.1682$ K, and $T_0 \sim 249.959$ K. Our VFT fit is also presented in the Supporting Information.

Querying the VFT fit at the four temperatures of the ice simulations, we can obtain estimates of the shear viscosity for the supercooled bulk liquid. These values are reported in Table S3 in the SI. We observe decreasing η_{bulk} with increasing temperature, although at 272 K the viscosity of TIP4P/Ice is significantly larger than experimental measurements of $\eta\ (273.15\text{ K}) = 1.8$ cP.[19] TIP4P/Ice is known to over-structure the liquid in order to obtain good melting points,[20] and this is likely to influence the liquid state viscosity as well. Figure S5 in the SI shows $\eta_{\text{qll}}(y,T)$ for both the basal and prismatic facets.

Two unitless, reduced viscosities can be defined for the quasi-liquid layer. The first, $\eta^*(y,T)$, relates the viscosity of the QLL to that of a bulk supercooled liquid of the same water model,

$$\eta^*(y,T) = \frac{\eta_{\text{qll}}(y,T)}{\eta_{\text{bulk}}(T)}, \tag{6}$$

while $\eta^*_m(y,T)$, relates the viscosity of the QLL to that of the same water model *at its melting*

point,

$$\eta_m^*(y,T) = \frac{\eta_{\mathrm{qll}}(y,T)}{\eta_{\mathrm{bulk}}(T_m)}. \tag{7}$$

If the viscosity of the QLL falls below the viscosity of the bulk liquid at the melting point, the dimensionless η_m^* will fall below 1. This allows us to compare the QLL to bulk liquid behavior when the viscosities and melting points are sensitive to the choice of water model. Reduced viscosities are shown in Fig. 2. There are three main observations that we can highlight from this data:

- Immediately adjacent to the ice / QLL interface, the viscosity of the QLL is 5–1000 times larger than that of bulk water. There is both a temperature and facet dependence for the viscosity proximal to the solid surface. The prismatic facet, with a higher density of solid-to-liquid hydrogen bonds,[3] exhibits larger surface-adjacent viscosities at all temperatures.

- Above 260 K, and at distances > 5 Å from the ice / QLL interface, the QLL viscosity has fallen *below* the viscosity of water at the melting point. This happens inside the QLL / vapor dividing surface in a region where the density and tetrahedrality have definite liquid-like character. Temperature and facet-dependence of η^* in this portion of the QLL is significantly weaker than in the surface-adjacent QLL.

- Templating of the liquid by the facet (i.e. energetically-preferred locations for liquid molecules) only extends to the water layer in direct contact with the solid. The layer of liquid in direct contact with the external vapor is significantly less viscous than water at the same temperature.

There are a few reasons why we might see the QLL viscosity display a strong dependence on the proximity to the solid interface. Close to the ice, the QLL is a partially-confined liquid, with half of the available space occupied by a hydrophilic solid surface. Nano-confined water in hydrophilic pores is known to have dramatically slowed translational[21] and reorientation dynamics.[22]

The close proximity to the ice surface also causes a structural templating on the liquid, with energetically preferred locations that are dictated by the underlying crystal. Motion of the water

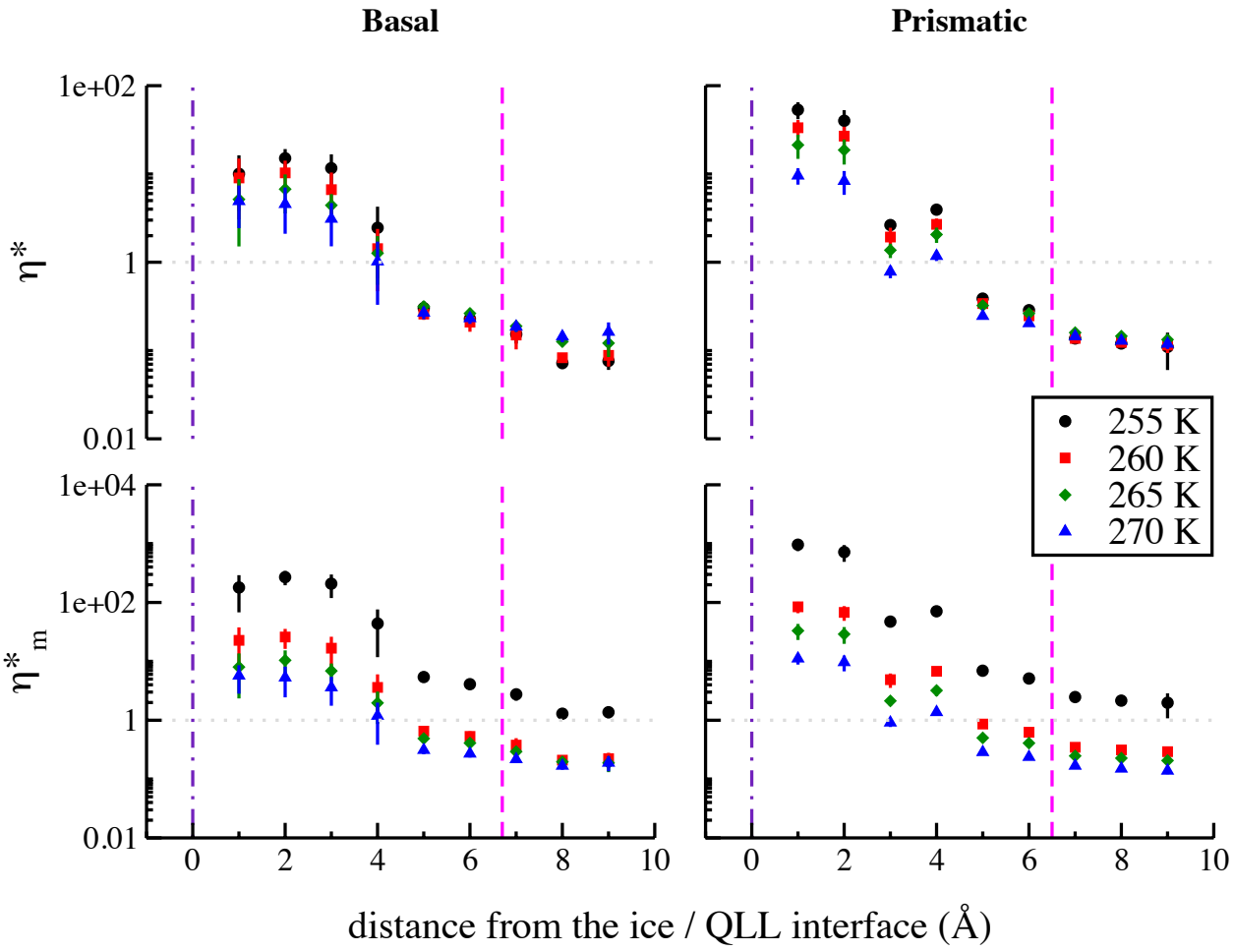

Figure 2: The reduced shear viscosities of the quasi-liquid layer at the basal (left) and prismatic (right) surfaces of ice-I_h. Values of η^* (upper panels) relate to viscosities of bulk supercooled liquids at the same temperature, while η^*_m (lower panels) relate to the viscosity of liquid water at T_m. The purple vertical dot-dashed line locates the ice / QLL interface, and pink dashed line indicates the dividing surface between the QLL and the vapor. Values of η^*_m below 1 (grey dotted line) indicate regions where the viscosity has fallen below the viscosity of water at the melting temperature. Error bars indicate 95% confidence intervals obtained from four statistically-independent samples for each data point.

molecules close to the solid involves hopping between these locations. Both the confinement and the templating may help explain the effective viscosities that are significantly larger than supercooled bulk water.

These arguments may also help explain the observation of very low viscosity in the vapor-adjacent layer. The density of the QLL at the liquid / vapor dividing surface is smaller than that of the supercooled bulk liquid, and therefore we expect a smaller resistance for the translational motion of molecules. In water at the liquid-vapor interface, both interface-parallel and perpendicular diffusion constants are known to be larger than bulk diffusion.[23] Here, we find that the in-plane diffusion parallel to the ice surface is the dominant mode of translational motion (see Fig. S6 in the Supporting Information).

Experimental probes of the viscosity of the QLL have been carried out using an optical microscope combined with differential interference contrast microscopy. Sazaki *et al.* imaged QLLs at the basal surface of ice.[24–29] Recently, Murata *et al.* have measured the surface tension-to-shear viscosity ratio for the basal exposed QLL.[26] They observed two separate QLL morphologies, partial wetting of the surface by a droplet and complete wetting by a thin liquid layer. They found the characteristic velocity ($V^* = \gamma/\eta$) of the thin film to be approximately 200 times smaller than that of bulk water at 0°C, indicating a relatively viscous QLL. Because the films for the Murata *et al.* measurements are significantly thicker than ours (9 nm vs. 0.7 nm), we see two ways to reconcile our simulations with these measurements. The thicker films may sample more of the solid-adjacent viscosities observed in our simulations, or the surface tension (γ) of the QLL is different than for bulk liquid water.

Lastly, comparing the shear viscosities close the ice / QLL interface for the basal and prismatic surfaces, we see that at all temperatures investigated $\eta_{\mathrm{qll}}^{\mathrm{prism}} > \eta_{\mathrm{qll}}^{\mathrm{basal}}$. This result agrees with our recent calculations of solid-liquid friction coefficients (κ), where we found $\kappa_{\mathrm{prism}} > \kappa_{\mathrm{basal}}$.[3] Conversely, close to the QLL / vapor interface, $\eta_{\mathrm{qll}}^{\mathrm{prism}}$ and $\eta_{\mathrm{qll}}^{\mathrm{basal}}$ come into agreement. Here, the shear viscosity of TIP4P/Ice is much smaller, varying from $\eta = 1.7$ cP to $\eta = 17.5$ cP with decreasing temperature. We conclude that the small coefficients of friction commonly associated with

ice surfaces is due almost entirely to the shear viscosity of water molecules near the QLL / vapor interface. This would agree with the recent measurements of the friction coefficient of steel-on-ice by Weber *et al.*[30] They attributed the observed friction coefficients to weakly hydrogen-bonded QLL / vapor molecules, whose population were found to increase with increasing temperature. This correlation matches the trend of decreasing friction coefficient with increasing temperature, until the point that the ice surface undergoes a plastic deformation. We note that our results and the results of Weber *et al.* are compatible for hydrophobic sliders and when the applied load is relatively small. For hydrophilic surfaces, or for loads which can impact the density of the QLL, other mechanisms may be involved.

In summary, we have performed molecular dynamics simulations of the exposed basal and prismatic surfaces of an ice-I_h crystal at four separate temperatures. Spontaneous QLL formation was observed at all temperatures > 255 K, and structural measurements of the width agree with other reported values. Using a temperature dependent model for the shear viscosity of bulk supercooled liquid water, we have provided estimates of the spatially resolved shear viscosity of the QLL at the basal and prismatic surfaces. We observe facet dependent viscosity close to the ice crystal which obeys a similar trend to our recently reported solid-liquid friction coefficients for these facets. At the QLL / vapor interface, the viscosity is 1,000 to 10,000 times smaller than at the ice / QLL interface, and we suggest that the small friction coefficients commonly observed for ice surfaces is due to this population of molecules.

Computational Methods: At temperatures ≤ 180 K, the basal face of ice-I_h presents stripes of protons and lone pairs to the vapor.[31–33] We have constructed our initial configurations from an ice-I_h unit cell proposed by Hirsch and Ojamäe (Structure 6) which, when replicated, reproduces these surface features.[34] We note that *all* simulations of ice structures have proton ordering on the length scale of the periodic box, but in order to reproduce proton surface striping with zero dipole crystals, we have utilized proton translational ordering on a smaller length scale than other ice studies. A more detailed description of how the crystals were constructed is given in references 3 and 35.

TIP4P/Ice[20] basal and prismatic ice-I_h primitive surfaces were constructed by replicating this unit cell and cleaving the crystal along the desired plane. Next, two mutually perpendicular cuts to the initial crystal face were made, and the resulting structure was then reoriented so that the desired crystal face was exposed normal to the *y* axis. The ice crystals were then replicated in the *x*- and *z*-dimensions to form large sheets exposing the desired face. The sheets were then replicated along the *y*-dimension until the basal crystal was 12 bilayers thick, and the prismatic crystal was replicated to a width approximating the width of the basal crystal. Dimensions and the number of molecules in each system are found in Table S1.

The *y*-dimension of the simulation box was then increased to 300 Å to allow for a surface premelt to form, and four replicas of each system were equilibrated to four temperatures, 255, 260, 265, and 270 K at 1 atm. The 32 resulting systems (16 for each facet) each exposed two interfaces, one toward positive *y* and the other towards negative *y*. Equilibration was conducted under a constant surface tension and temperature (NγT) ensemble, allowing the *x*- and *z*-dimensions of the simulation cell to relax and alleviate any crystal strain. Following this, the systems were equilibrated for 1 ns in the canonical ensemble (NVT), and lastly for 1 ns in the microcanonical (NVE) ensemble. Once equilibration was complete, four 500 ps production simulations in a microcanonical (NVE) ensemble were performed for each system, with positions and velocities recorded every 1 ps. The temperature of each system was observed to be stable during these production simulations. For all simulations, non-bonded interactions were cut-off at 12 Å and electrostatics were handled using the damped-shifted force real-space electrostatic kernel.[36] All simulations were performed using OpenMD,[37,38] with a time step of 2 fs and periodic boundary conditions in all three dimensions.

For the supercooled bulk liquid simulations, a cubic box of 4,000 water molecules was constructed and replicas were equilibrated to 255, 260, 265, and 270 K at 1 atm. System sizes and corresponding densities are presented in Table S2. Once the liquid boxes were equilibrated, four successive 1 ns simulations were performed in the microcanonical (NVE) ensemble. For bulk liquid simulations, positions and velocities were stored every 100 fs.

To map the temperature dependence of the shear viscosity in supercooled bulk liquid, a box containing $16,000$ TIP4P/Ice molecules with dimensions $L_x = 51.22$ Å, $L_y = 51.22$ Å, and $L_z = 200.87$ Å was stabilized for 1 ns at a temperature of 262.5 K and pressure of 1 atm. The velocity shearing and scaling variant of reverse non-equilibrium molecular dynamics (VSS-RNEMD) was used to simultaneously impose nonphysical kinetic energy and momentum fluxes. VSS-RNEMD moves were attempted every timestep in order to minimize the magnitude of the individual kicks. Thermal and velocity gradients were allowed to stabilize for 1 ns, before data collection was taken over a subsequent 1 ns simulation.

Acknowledgement

Support for this project was provided by the National Science Foundation under grant CHE-1663773. Computational time was provided by the Center for Research Computing (CRC) at the University of Notre Dame.

Supporting Information Available

Details about the models used to carry out the simulations, full density and tetrahedrality profiles, distributions of tetrahedrality values, temperature dependence of the viscosity of bulk supercooled water, diffusion constants (both three dimensional and in-plane), and unreduced QLL viscosities not shown above.

References

(1) Kietzig, A. M.; Hatzikiriakos, S. G.; Englezos, P. Ice Friction: The Effects of Surface Roughness, Structure, and Hydrophobicity. *J. Appl. Phys.* **2009**, *106*, 024303.

(2) Kietzig, A. M.; Hatzikiriakos, S. G.; Englezos, P. Physics of Ice Friction. *J. Appl. Phys.* **2010**, *107*, 081101.

(3) Louden, P. B.; Gezelter, J. D. Friction at Ice-Ih/Water Interfaces Is Governed by Solid/Liquid Hydrogen-Bonding. *J. Phys. Chem. C* **2017**, *121*, 26764–26776.

(4) Kroes, G. J. Surface Melting of the (0001) Face of TIP4P Ice. *Surf. Sci.* **1992**, *275*, 365–382.

(5) Nada, H.; Furukawa, Y. Anisotropy in Structural Phase Transitions at Ice Surfaces: A Molecular Dynamics Study. *Appl. Surf. Sci.* **1997**, *121*, 445–447.

(6) Nada, H.; van der Eerden, J. P. J. M. An Intermolecular Potential Model for the Simulation of Ice and Water Near the Melting Point : A Six-Site Model of H_2O. *J. Chem. Phys.* **2003**, *118*, 7401–7413.

(7) Ikeda-Fukazawa, T.; Kawamura, K. Molecular-Dynamics Studies of Surface of Ice Ih. *J. Chem. Phys.* **2004**, *120*, 1395–1401.

(8) Conde, M. M.; Vega, C.; Patrykiejew, A. The Thickness of a Liquid Layer on the Free Surface of Ice as Obtained From Computer Simulation. *J. Chem. Phys.* **2008**, *129*, 014702.

(9) Neshyba, S.; Nugent, E.; Roeselová, M.; Jungwirth, P. Molecular Dynamics Study of Ice - Vapor Interactions via the Quasi-Liquid Layer. *J. Phys. Chem. C* **2009**, *113*, 4597–4604.

(10) Pfalzgraff, W.; Neshyba, S.; Roeselova, M. Comparative Molecular Dynamics Study of Vapor-Exposed Basal, Prismatic, and Pyramidal Surfaces of Ice. *J. Phys. Chem. A* **2011**, *115*, 6184–6193.

(11) Gladich, I.; Pfalzgraff, W.; Maršálek, O.; Jungwirth, P.; Roeselová, M.; Neshyba, S. Arrhenius Analysis of Anisotropic Surface Self-Diffusion on the Prismatic Facet of Ice. *Phys. Chem. Chem. Phys.* **2011**, *13*, 19960.

(12) Gladich, I.; Oswald, A.; Bowens, N.; Naatz, S.; Rowe, P.; Roeselova, M.; Neshyba, S. Mechanism of Anisotropic Surface Self-Diffusivity at the Prismatic Ice-Vapor Interface. *Phys. Chem. Chem. Phys.* **2015**, *17*, 22947–58.

(13) Errington, J.; Debenedetti, P. Relationship Between Structural Order and the Anomalies of Liquid Water. *Nature* **2001**, *409*, 318–321.

(14) Nada, H.; Furukawa, Y. Anisotropic Properties of Ice / Water Interface : A Molecular Dynamics Study. *Jpn. J. Appl. Phys.* **1995**, *34*, 583–588.

(15) Michaelides, A.; Slater, B. Melting the Ice One Layer at a Time. *Proc. Natl. Acad. Sci. U.S.A.* **2017**, *114*, 195–197.

(16) Vanegas, J. M.; Torres-Sánchez, A.; Arroyo, M. Importance of Force Decomposition for Local Stress Calculations in Biomembrane Molecular Simulations. *J. Chem. Theory Comput.* **2014**, *10*, 691–702.

(17) Kuang, S.; Gezelter, J. D. Velocity Shearing and Scaling RNEMD: A Minimally Perturbing Method for Simulating Temperature and Momentum Gradients. *Mol. Phys.* **2012**, *110*, 691–701.

(18) Debenedetti, P. G.; Stanley, H. E. Supercooled and Glassy Water. *Physics Today* **2003**, 40–46.

(19) Dehaoui, A.; Issenmann, B.; Caupin, F. Viscosity of Deeply Supercooled Water and its Coupling to Molecular Diffusion. *Proc. Natl. Acad. Sci. U.S.A.* **2015**, *112*, 12020–12025.

(20) Abascal, J. L. F.; Sanz, E.; Fernández, R. G.; Vega, C. A Potential Model for the Study of Ices and Amorphous Water: TIP4P/Ice. *J. Chem. Phys.* **2005**, *122*, 234511.

(21) Milischuk, A. A.; Ladanyi, B. M. Structure and Dynamics of Water Confined in Silica Nanopores. *J. Chem. Phys.* **2011**, *135*.

(22) Laage, D.; Thompson, W. H. Reorientation Dynamics of Nanoconfined Water: Power-Law Decay, Hydrogen-Bond Jumps, and Test of a Two-State Model. *J. Chem. Phys.* **2012**, *136*, 044513.

(23) Liu, P.; Harder, E.; Berne, B. J. On the Calculation of Diffusion Coefficients in Confined Fluids and Interfaces with an Application to the Liquid Vapor Interface of Water. *J. Phys. Chem. B* **2004**, *108*, 6595–6602.

(24) Sazaki, G.; Zepeda, S.; Nakatsubo, S.; Yokomine, M.; Furukawa, Y. Quasi-Liquid Layers on Ice Crystal Surfaces are Made Up of Two Different Phases. *Proc. Natl. Acad. Sci. U.S.A.* **2012**, *109*, 1052–1055.

(25) Sazaki, G.; Asakawa, H.; Nagashima, K.; Nakatsubo, S.; Furukawa, Y. How Do Quasi-Liquid Layers Emerge From Ice Crystal Surfaces? *Cryst. Growth Des.* **2013**, *13*, 1761–1766.

(26) Murata, K. I.; Asakawa, H.; Nagashima, K.; Furukawa, Y.; Sazaki, G. In Situ Determination of Surface Tension-to-Shear Viscosity Ratio for Quasiliquid Layers on Ice Crystal Surfaces. *Phys. Rev. Lett.* **2015**, *115*, 256103.

(27) Murata, K.-i.; Asakawa, H.; Nagashima, K.; Furukawa, Y.; Sazaki, G. Thermodynamic Origin of Surface Melting on Ice Crystals. *Proc. Natl. Acad. Sci. U.S.A.* **2016**, *113*, E6741–E6748.

(28) Asakawa, H.; Sazaki, G.; Nagashima, K.; Nakatsubo, S.; Furukawa, Y. Two Types of Quasi-Liquid Layers on Ice Crystals are Formed Kinetically. *Proc. Natl. Acad. Sci. U.S.A.* **2016**, *113*, 1749–1753.

(29) Inomata, M.; Murata, K. I.; Asakawa, H.; Nagashima, K.; Nakatsubo, S.; Furukawa, Y.; Sazaki, G. Temperature Dependence of the Growth Kinetics of Elementary Spiral Steps on Ice Basal Faces Grown from Water Vapor. *Cryst. Growth Des.* **2018**, *18*, 786–793.

(30) Weber, B.; Nagata, Y.; Ketzetzi, S.; Tang, F.; Smit, W. J.; Bakker, H. J.; Backus, E. H.; Bonn, M.; Bonn, D. Molecular Insight into the Slipperiness of Ice. *J. Phys. Chem. Lett.* **2018**, *9*, 2838–2842.

(31) Groenzin, H.; Li, I.; Buch, V.; Shultz, M. J. The Single-Crystal, Basal Face of Ice Ih Investigated With Sum Frequency Generation. *J. Chem. Phys.* **2007**, *127*, 214502.

(32) Buch, V.; Groenzin, H.; Li, I.; Shultz, M. J.; Tosatti, E. Proton Order in the Ice Crystal Surface. *Proc. Natl. Acad. Sci. U.S.A.* **2008**, *105*, 5969–5974.

(33) Nojima, Y.; Suzuki, Y.; Takahashi, M.; Yamaguchi, S. Proton Order toward the Surface of Ice Ih Revealed by Heterodyne-Detected Sum Frequency Generation Spectroscopy. *J. Phys. Chem. Lett.* **2017**, *8*, 5031–5034.

(34) Hirsch, T. K.; Ojamäe, L. Quantum-Chemical and Force-Field Investigations of Ice Ih: Computation of Proton-Ordered Structures and Prediction of Their Lattice Energies. *J. Phys. Chem. B* **2004**, *108*, 15856–15864.

(35) Louden, P. B.; Gezelter, J. D. Simulations of Solid-Liquid Friction at Ice-Ih/Water Interfaces. *J. Chem. Phys.* **2013**, *139*, 194710.

(36) Fennell, C. J.; Gezelter, J. D. Is the Ewald Summation Still Necessary? Pairwise Alternatives to the Accepted Standard for Long-Range Electrostatics. *J. Chem. Phys.* **2006**, *124*, 234104.

(37) Meineke, M. A.; Vardeman, C. F.; Lin, T.; Fennell, C. J.; Gezelter, J. D. OOPSE: An Object-Oriented Parallel Simulation Engine for Molecular Dynamics. *J. Comput. Chem.* **2005**, *26*, 252–271.

(38) Gezelter, J. D.; Bhattarai, H.; Niedhart, S.; Louden, P. B.; Lin, T.; Vardeman, C. F.; Fennell, C. J.; Meineke, M. A.; Kuang, S.; Lamichane, M. et al. OpenMD, an Open Source Engine for Molecular Dynamics. 2016; `http://openmd.org`.